THE ASTROPHYSICAL JOURNAL, 486:799–809, 1997 September 10

MULTIWAVELENGTH MONITORING OF THE BL LACERTAE OBJECT PKS 2155−304 IN 1994 MAY. III. PROBING THE INNER JET THROUGH MULTIWAVELENGTH CORRELATIONS

C. MEGAN URRY,[1] ALDO TREVES,[2,3] LAURA MARASCHI,[4] HERMAN L. MARSHALL,[5] TSUNEO KII,[6] GREG MADEJSKI,[7] STEVE PENTON,[8] JOSEPH E. PESCE,[1] ELENA PIAN,[1] ANNALISA CELOTTI,[2,11] R. FUJIMOTO,[6] F. MAKINO,[6] C. OTANI,[6] R. M. SAMBRUNA,[7] K. SASAKI,[6] J. M. SHULL,[8] PAUL S. SMITH,[9] T. TAKAHASHI,[6] AND M. TASHIRO[10]

Received 1996 July 12; accepted 1997 April 21

ABSTRACT

In 1994 May, the BL Lac object PKS 2155−304 was observed continuously for ∼10 days with the *International Ultraviolet Explorer* and the *Extreme Ultraviolet Explorer* and for 2 days with *ASCA*, as well as with *ROSAT* and with ground-based radio, infrared, and optical telescopes. The light curves show a well-defined X-ray flare followed by a broader, lower amplitude extreme-ultraviolet flare ∼1 day later and a broad, low-amplitude UV flare ∼2 days later. X-ray fluxes obtained at three well-separated times the preceding week indicate at least one previous flare of comparable amplitude or perhaps ongoing stochastic X-ray variations, and additional rapid variability was seen at the beginning of the *IUE* observation, when extremely sharp changes in UV flux occurred. The X-ray flux observed with *ASCA* flared by a factor of ∼2 in about half a day and decayed roughly as fast. In contrast, the subsequent UV flare had an amplitude of only ∼35% and lasted longer than 2 days.

Assuming that the X-ray, EUV, and UV events are associated, the lags, the decrease of amplitude with wavelength, and the broadening of the temporal profile with wavelength are all qualitatively as expected for synchrotron emission from an inhomogeneous, relativistic jet. Because of the high quality of the data, we can rule out that the observed flares were caused by either a Fermi-type shock acceleration event or a pair cascade in a homogeneous synchrotron-emitting region. A homogeneous region is still possible if there was an instantaneous ($t \ll$ hours) injection of high-energy electrons that emit first at X-ray energies. Alternatively, the data are consistent with a compression wave or other disturbance crossing a region with stratified particle energy distributions. This kind of situation is expected to occur behind a shock front and/or in an inhomogeneous jet. The present light curves are in sharp contrast to the multiwavelength variability observed in 1991 November, when the amplitude was wavelength independent and the UV lagged the X-rays by less than ∼3 hr. This means that the origin of rapid multiwavelength variability in this blazar is complex, involving at least two different modes.

Subject headings: BL Lacertae objects: individual (PKS 2155−304) — galaxies: active — galaxies: jets — ultraviolet: galaxies — X-rays: galaxies

1. INTRODUCTION

Multiwavelength observations have established that the continuum emission from BL Lac objects is almost certainly produced by high-energy particles in a relativistic jet (Bregman, Maraschi, & Urry 1987). Furthermore, the recent detection of high-energy gamma rays from many blazars confirms that the emitted radiation is relativistically beamed along the jet axis (Maraschi, Ghisellini, & Celotti 1992; Dermer & Schlickeiser 1993). How the plasma is accelerated to relativistic bulk velocity and how radiating particles within the plasma are accelerated to high energies remain essentially unknown.

The multiwavelength spectra of BL Lac objects are remarkably smooth and steepen progressively from radio to X-ray wavelengths, with the emitted power per decade peaking between 10^{13} and 10^{16} Hz (Giommi, Ansari, & Micol 1995; Sambruna, Maraschi, & Urry 1996). The primary mechanism for this emission is most likely synchrotron radiation. There is a separate, harder component peaking near (or in some cases well above) 1 GeV (von Montigny et al. 1995), which is probably due to inverse Compton scattering of lower energy photons, either synchrotron photons within the jet or other UV photons external to the jet (see, e.g., Maraschi, Ghisellini, & Celotti 1994, and references therein).

One of the key problems in interpreting blazar spectra is explaining the gradual steepening of the synchrotron power law. One possibility is that the emission comes from a homogeneous region, in which case the increasing effec-

[1] Space Telescope Science Institute, 3700 San Martin Drive, Baltimore, MD 21218. The Space Telescope Science Institute is operated by the Association of Universities for Research in Astronomy, Inc., under contract with the National Aeronautics and Space Administration. cmu@stsci.edu.

[2] International School for Advanced Studies (SISSA), via Beirut 2–4, I-34014 Trieste, Italy.

[3] Dipartimento di Fisica, Università degli studi di Milano, sede di Como, via Lucini, I-22100 Como, Italy.

[4] Osservatorio Astronomico di Brera, via Brera 28, I-20121 Milano, Italy.

[5] Eureka Scientific, Inc., Suite 100, 2452 Delmer Street, Oakland, CA 94602.

[6] Institute for Space and Astronautical Science, 3-1-1 Yoshinodai, Sagamihara, Kanagawa 229, Japan.

[7] Laboratory for High Energy Astrophysics, Code 666, Goddard Space Flight Center, Greenbelt MD 20771.

[8] Joint Institute for Laboratory Astrophysics, University of Colorado, Campus Box 440, Boulder, CO 80309-0440.

[9] Steward Observatory, University of Arizona, Tucson, AZ 85721.

[10] Department of Physics, School of Science, University of Tokyo, Bunkyo-ku, Tokyo 113, Japan.

[11] Institute of Astronomy, Madingley Road, Cambridge, CB3 0HA, England, UK.

tiveness of energy losses at higher energies can steepen the spectrum. Alternatively, the particle spectra and other physical quantities may vary along the jet (i.e., the jet is inhomogeneous) so that progressively more extended regions in the jet effectively emit at increasing wavelengths. Either possibility is consistent with single-epoch multiwavelength spectra.

Spectral variability at X-ray wavelengths is common, with spectra typically hardening with increasing intensity (Sambruna et al. 1994, and references therein). Multiwavelength variability can provide strong clues about the processes of particle injection acceleration and diffusion in the emission region(s) and/or about the relative location of emission regions for different spectral bands. That is, multiepoch multiwavelength data do constrain (and perhaps now overconstrain) current blazar models.

Accordingly, we carried out comprehensive multiwavelength monitoring of the BL Lac object PKS 2155−304 in 1991 November (Edelson et al. 1995; Smith et al. 1992; Urry et al. 1993; Brinkmann et al. 1994; Courvoisier et al. 1995). PKS 2155−304 is the brightest blazar at UV wavelengths and is also very bright in the X-ray and optical bands, making it the best candidate for monitoring at short wavelengths. The 3.5 days of overlapping *ROSAT* and *International Ultraviolet Explorer* data from 1991 November showed very rapid, highly correlated variability, with a secular decrease superposed with multiple peaks of roughly equal amplitude in optical, UV, and X-ray bands, and with a possible 2–3 hr delay of the UV with respect to X-ray light curve (Edelson et al. 1995). The rapidity of the variations, the lack of dependence of the variability amplitude upon wavelength, and the short lag were somewhat unexpected for synchrotron emission from an inhomogeneous jet (see, e.g., Celotti, Maraschi, & Treves 1991); the repetitive peaks across the intensity decline were also intriguing.

We therefore planned a second, longer monitoring campaign with even more extensive wavelength coverage, involving *IUE*, the *Extreme Ultraviolet Explorer* (*EUVE*), *ROSAT*, and *ASCA*. The observations were designed to resolve the fastest timescale variability, to follow the light curve (at high temporal resolution) considerably longer than in 1991, and to improve the measurement of the UV–X-ray cross-correlation. This second campaign took place in 1994 May. PKS 2155−304 was observed with *IUE* and *EUVE* for 10 and 9 days, respectively, and for 2 days with *ASCA*. A few *ROSAT* observations were also made just prior to the *ASCA* pointing.

Here we present the multiwavelength results from the 1994 May campaign. The observations and resulting light curves are described briefly in § 2, and a multiwavelength cross-correlation analysis is presented in § 3. In § 4, we discuss possible interpretations of the multiwavelength results. Full results in each wavelength range and details of the data reduction and analyses are presented in separate papers (UV, Pian et al. 1997; EUV, Marshall et al. 1997; X-ray, Kii et al. 1997; ground-based radio to optical, Pesce et al. 1997). Conclusions are summarized in § 5.

2. OBSERVATIONS AND RESULTS

In the following, we describe briefly the 1994 multiwavelength observations of PKS 2155−304, particularly those made with high time resolution in the UV, EUV, and X-ray energy bands. We refer to the aformentioned papers for complete presentations. Dates are reported in UT throughout the text, and in both UT and MJD (≡JD − 2,440,000) in the figures, taking into account that MJD 9,487.5 corresponds to 1994 May 15, 0000 UT.

2.1. *UV Light Curves*

The UV data were taken with *IUE* between 1994 May 15 and 25 with only a few short gaps due to Earth occultation. The LWP (long wavelength) and SWP (short wavelength) cameras were exposed alternately, with typical exposure times of 25 and 55 minutes, respectively, in phase with the 96 minute *ROSAT* orbital period. Spectra were extracted using TOMSIPS (Ayres 1993; Ayres et al. 1995), a modified version of the signal-weighted extraction technique (Kinney, Bohlin, & Neill 1991) adapted for the *IUE* Final Archive. Spectra were dereddened assuming $A_V = 0.1$ mag and then fitted with power laws separately in the LWP (2100–2800 Å) and SWP (1230–1950 Å) wavelength ranges. Light curves were constructed from the fitted fluxes at 2800 and 1400 Å; the LWP fluxes have larger uncertainties because of the smaller effective range of the fits, given the noise below ∼2400 Å and the scattered light above ∼2800 Å. The mean fluxes for the *IUE* observations were $(7 \pm 1) \times 10^{-14}$ ergs cm^{-2} s^{-1} Å^{-1} for the LWP and $(15 \pm 2) \times 10^{-14}$ ergs cm^{-2} s^{-1} Å^{-1} for the SWP. Further information about the *IUE* results is given by Pian et al. (1997).

In Figure 1, we show the combined SWP/LWP light curves, created by normalizing separately to the individual mean fluxes; the effective time resolution of the combined light curve is ∼48 minutes. The two light curves are very similar, with a prominent flare centered on May 21. The amplitude of this flare is ∼35% in both cameras (for amplitude defined as $\Delta F/F_{\rm initial}$) and the duration (FWHM) is ∼2 days. The structure of the flare is also similar in both cameras, with comparable rise and decay times and with a flat plateau at the peak, but with a small shoulder during the rise. The spectral index in the short, long, and combined wavelength ranges is remarkably constant across the flare. Some smaller amplitude variability (5%–10%) is also seen in both cameras throughout the observation.

In addition, there is a dramatic event at the very beginning of the observation: a fast rise, followed by a dip, and another fast rise to the mean flux level. These initial flares represent the fastest ever seen at UV wavelengths in an extragalactic object. The doubling timescale, defined as $\tau_d \equiv (F_{\rm initial}/\Delta F)\Delta t$, is ∼1 hr for the LWP flux, comparable to the timescale of the fastest variations seen at X-ray and gamma-ray wavelengths. (For the fast UV and X-ray variations discussed here, the *e*-folding times are similar.) The doubling time for the central flare is much longer: $\tau_d \sim 3$–4 days. Throughout the observation, the spectral index varies significantly but by a small amount (except during the first flare, when the variability timescale is less than the temporal resolution; Pian et al. 1997).

2.2. *EUV Light Curve*

The *EUVE* satellite was pointed at PKS 2155−304 for 9 days, from 1994 May 11 to 20, with the Deep Survey Spectrometer. The primary goal of this observation was to try a new method for measuring polarization in the soft X-ray band, as well as to obtain a high-quality EUV spectrum of this BL Lac object (Königl et al. 1995; see also Fruscione et al. 1994). The long integration time required

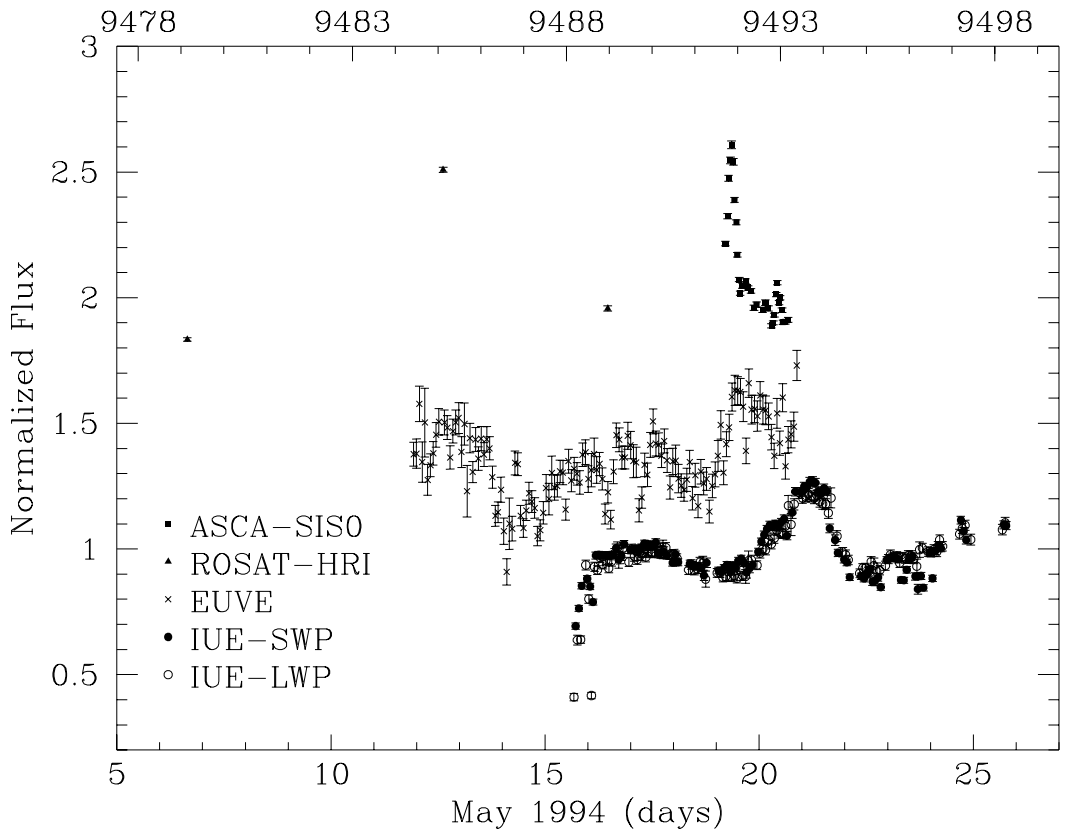

FIG. 1.—Multiwavelength light curves of PKS 2155−304 from the 1994 May campaign. The *ASCA*, *ROSAT*, and *EUVE* fluxes are averages over one orbit. Each light curve has been normalized to its mean intensity; for the *IUE* data, this was computed after discarding the first six flux points from both SWP and LWP light curves. For clarity, the EUV and X-ray light curves have been shifted vertically by 0.4 and 1.1, respectively. Modified Julian Dates are reported on the upper axis (MJD 9,487.5 = 1994 May 15, 0000 UT).

for a good signal-to-noise ratio (PKS 2155−304 is one of only a handful of extragalactic objects that can even be detected with *EUVE*) resulted in the excellent long-term light curve discussed here. Additional details and results are given by Marshall et al. (1997).

The normalized EUV light curve is shown in Figure 1. The data are binned on the orbital timescale (96 minutes), and each bin represents 500–1000 s of exposure. All variations appear to be resolved; that is, 300 s light curves reveal no flares that are not also apparent in the longer binned data. Although the errors on the fluxes are larger than for the UV light curve, the EUV light curve shows a similar structure. In particular, a sharp rise occurs around May 19, with a $\sim$50% amplitude and $\sim$1–2 day duration, very similar to the UV flare occurring about a day later. Also, the minimum on May 14 resembles (within the large errors) the initial event seen on May 16 with *IUE*. This is shown with an expanded scale in Figure 2, and with the EUV light curve shifted by 1 day, corresponding to the peak in the EUV-UV cross-correlation function (see § 3).

2.3. *X-Ray Light Curve*

The *ASCA* satellite was pointed at PKS 2155−304 for 2 days, from 0430 UT on May 19 to 0755 UT on May 21. The goal of the observation was to study the energy dependence of fast X-ray variability and to follow the evolution of the X-ray spectrum over the wide energy band of 0.5–8 keV; these issues are discussed in detail by Kii et al. (1997). Data were accumulated with the two SIS and two GIS focal-plane detectors, which have overlapping but slightly different energy ranges (Tanaka, Inoue, & Holt 1994).

The results presented here are from the SIS detectors, which have wider energy coverage and better energy resolution than the GIS (which yield equivalent results in any case; Kii et al. 1997). The SIS detectors were operated in 1-CCD faint mode for high–bit-rate data and in 1-CCD bright mode for medium–bit-rate data. The data extraction followed the standard recommendations of the *ASCA* instrument teams. Since the count rate of the background and its fluctuations are negligible compared with the count rate from PKS 2155−304, we performed no background subtraction for the timing analysis, so as to avoid any artificial effects.

The normalized X-ray light curve from the *ASCA* SIS0 CCD is shown in Figure 1. A pronounced high-amplitude flare occurs at the beginning of the observation. The observed 0.5–8 keV flux is 3.3×10^{-10} ergs cm^{-2} s^{-1} at the peak and 1.5×10^{-10} ergs cm^{-2} s^{-1} at the minimum. The shape of the flare is approximately symmetric in time. The doubling time for the decay is $\tau_d \sim 0.5$ day; its duration is less clear since the flare may well have begun before the start of the observation. The observed part of the flare rise is symmetric with respect to the decay, so, assuming symmetry, we estimate that the flare duration (FWHM) is $\sim$1 day. Toward the end of the decay two smaller flares are visible. The cross-correlation between the 0.5–1 and 2.2–8 keV bands shows clear evidence that the hard X-rays lead the soft X-rays by $\sim$5 ks (Kii et al. 1997).

We analyzed the SIS0 spectra accumulated in each orbit, fitting a power-law model with fixed Galactic absorption

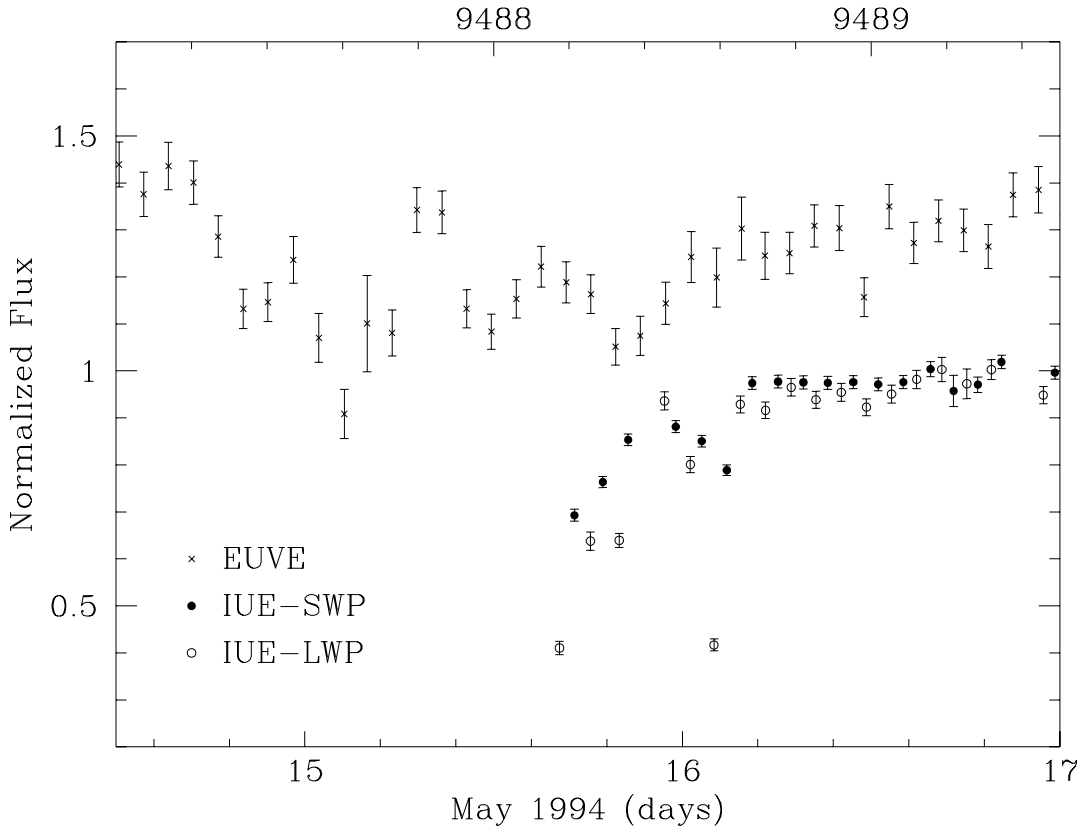

FIG. 2.—Expanded view of part of the normalized *EUVE* and *IUE* light curves, with the former shifted forward by its lead time, 1 day, and upward by 0.35, for clarity. Although the *EUVE* data are noisy, variations similar to the initial UV flares can be seen, although they are much smaller in amplitude and not at the same lag as the central flare. Modified Julian Dates are reported on the upper axis.

($N_{\rm H\,I} = 1.77 \times 10^{20}$ cm^{-2}; Stark et al. 1992). For the energy range 0.5–8 keV, the energy spectral index varied from $\alpha = 1.29 \pm 0.02$ at the beginning of the observation ($F_{1\,\rm keV} = 44.9 \pm 0.4$ μJy), to $\alpha = 1.25 \pm 0.02$ just before the peak ($F_{1\,\rm keV} = 58.3 \pm 0.5$ μJy), to 1.80 ± 0.02 near the end ($F_{1\,\rm keV} = 32.4 \pm 0.4$ μJy, more or less the faintest state). The observed spectral change is similar to previous observations of the spectrum's hardening (softening) with increasing (decreasing) intensity (Treves et al. 1989; Sembay et al. 1993) and is consistent with the observation that the hard X-rays lead the soft X-rays.

PKS 2155−304 was also observed in soft X-rays with the *ROSAT* HRI for three short (one orbit) periods, on 1994 May 9, 12, and 16, just before the bulk of the multiwavelength campaign. The HRI is sensitive in the energy range ~0.1–2.4 keV but provides little spectral information. The data were reduced using the standard *ROSAT* HRI criteria. Source counts were extracted from a region 30″ in radius, while the background counts were extracted from an annulus with inner and outer radii of 3′ and 5′; the background level is typically 0.3% of the source counts. No other point sources at a level greater than 1% of the intensity of PKS 2155−304 were present in the HRI field of view.

Examination of the resulting light curve (Fig. 1) reveals large-amplitude variability from one *ROSAT* observation to the next, with count rates of 5.12 ± 0.05, 9.83 ± 0.07, and 5.98 ± 0.07 counts s^{-1}, chronologically. There is no significant variability within each 2000 s observation; for time intervals between 400 and 2000 s, there is less than 3.1% peak-to-peak variability (the statistical uncertainty in each bin is less than 2.5%). This is close to the systematic limit due to the residual uncalibrated nonuniformities of the HRI; while the estimate of the relative variability amplitude on timescales of 400 s or longer is probably reliable at the ~2% level, systematic effects due to the wobble of the spacecraft every 400 s and nonuniformities in the photocathode of the HRI limit the determination of the variability amplitude to an estimated 5% (S. Snowden 1996, private communication). The resulting background-subtracted count rates were converted to flux by using an absorbed power-law model with power-law (energy) index of $\alpha = 1.5$, as measured by *ASCA* (Kii et al. 1997), and the Galactic column density $N_{\rm H\,I} = 1.36 \times 10^{20}$ cm^{-2} (Lockman & Savage 1995). The resulting unabsorbed 1 keV flux densities are 24.6 ± 0.3, 47.2 ± 0.4, and 28.7 ± 0.4 μJy.

While the *ROSAT* sampling is modest, the HRI light curve clearly indicates large-amplitude variability in the soft X-ray range in the first weeks of 1994 May on a timescale of several days, with an absence of such variability on timescales of 400–2000 s. Although no variations were resolved with *ROSAT*, the HRI data suggest that the flare seen with *ASCA* was not an isolated event.

3. COMPARISON OF LIGHT CURVES IN DIFFERENT BANDS

3.1. *UV, EUV, and X-Ray Correlations*

The most striking feature of the multiwavelength light curves is the well-defined large-amplitude flare seen with *ASCA*. The X-ray coverage is unfortunately very limited and the longer wavelength light curves do not overlap completely, so we cannot be certain, even for this extensive data

set, that the X-ray flare on May 19 corresponds to the UV flare on May 21. In making this identification, the *EUVE* data are critical. The wavelength range of *EUVE* (60–90 Å, with effective wavelength ∼75 Å) is close to the geometric mean of the *ASCA* and *IUE* ranges, and the intermediate properties of the *EUVE* flare (the time at which the flare is centered, its amplitude, and its duration) support our assumption that the correlations and delays derived below represent the real propagation of a flare from short to long wavelengths rather than the coincidental alignment of unassociated events.

We computed formal cross-correlations using the discrete correlation function (DCF; Edelson & Krolik 1988, with modified normalization given by J. H. Krolik 1996, private communication). This method samples time intervals for which data in both light curves exist, without interpolation. The input light curves were the SIS0 light curve binned at 96 minutes to improve the statistics, the *EUVE* light curve binned also at 96 minutes, and the combined normalized *IUE* SWP and LWP light curves at approximately 48 minute resolution.

The resulting cross-correlations of the *ASCA-IUE* and *EUVE-IUE* light curves are shown in Figures 3*a* and 3*b*, and the lags are summarized in Table 1. (The cross-correlation of the *EUVE* and *ASCA* light curves does not yield useful results, because of the very short overlap.) The UV light curve is strongly correlated with each of the other two, with the UV lagging the X-ray by ∼2 days and lagging the EUV by ∼1 day. In the latter case, not only do the broad flares line up with these delays, but also the rapid increase at the beginning of the *IUE* observation (May 15) could correspond (within about half a day) to dips in the *EUVE* light curve (Fig. 2). Note that this UV flare is undersampled even with the LWP, which represents the shortest integration time (the SWP time bins are twice as long). Intrinsically rapid variations integrated over longer time periods will have lower apparent amplitudes, as observed. (This does not apply to the flare of May 19–21, which is well resolved.)

The amplitudes and shapes of the flares differ in the various wavelength bands, as summarized in Table 1. The flare is sharpest at X-ray wavelengths, lasting no longer than a day, and is symmetric, with $\tau_d \sim 0.5$ day (the *e*-folding times are similar). At UV wavelengths, the rise is clearly slower, with some possible structure—the rise and fall times are $\tau_d \sim 4$ days and $\tau_d \sim 2.5$ days, respectively—and the flare lasts 2.5 days. (Given the uncertainties, the UV light curve could represent a single flare with a flat top or two separate flares. In the analysis below, we assume a single flare for simplicity.) The increase in X-ray flux is roughly a factor of 2, while the UV increase is ∼35% in amplitude. The uncertainties in the EUV light curve are larger as a result of the low count rates for PKS 2155−304 (as for any extragalactic object), so the flare's shape is not well determined. The flare amplitude is clearly lower than for the X-ray and more like the UV, with a value near ∼50%. The EUV rise time is $\tau_d \sim 1$ day, faster than in the UV; the decay time is less well determined to be ∼2 days but within the uncertainties could be as long as 5 days. The duration of the EUV flare appears to be roughly 1.5 days, but because the *EUVE* observation ends at that point, it could be longer.

3.2. *Comparison of Optical Flux and Polarization with UV Light Curves*

In general, the optical light curves are less well sampled than the shorter wavelength light curves, but they have much longer time coverage (Pesce et al. 1997). The comparison of the *V*-band and UV light curves in Figure 4 makes clear that the two total flux curves could have comparable timescales and amplitudes. The coverage was too sparse to associate any variations directly with the rapid initial UV flare on May 16, but a few days later an increase of ∼0.3 mag (∼30%) is seen in both the *V* and *R* bands, corresponding almost exactly to the UV flare of May 21, with little or no lag ($\lesssim 1$ day). Toward the end of the campaign, on May 25, the *BVRI* fluxes show a slow increase along with the UV, with the amplitude increasing toward the blue ($\Delta m \sim 0.01$ mag for *R* and *I*, $\Delta m \sim 0.1$–0.2 mag for *V* and *B*). Thus the optical and UV fluxes are generally well correlated, as observed previously.

The variability in polarized *V*-band flux is much larger than in unpolarized flux (Fig. 4). Although the sampling is still sparse, the polarized flux dips dramatically when the UV flux is low during the initial flare. Later, a strong flare in polarized *V*-band flux occurs at roughly the same time as the central UV/EUV/X-ray flare, peaking perhaps 1 day after the peak of the X-ray flare and the onset of the *EUVE* flare, and at approximately the same time as the UV flare. The coincidence of these two features, the initial and central flares, suggests a very close connection between the polarized optical flux and the UV flux. If so, we can infer that the initial UV variability was indeed a dip from the mean intensity level, rather than a flare from a lower state.

3.3. *Broadband Spectral Energy Distributions*

As a complementary view to the light curves in Figure 1, we show in Figure 5 four simultaneous broadband spectral

TABLE 1

MULTIWAVELENGTH VARIABILITY TIMESCALES

Band	$\nu_{\rm eff}$ (Hz)	τ_d (days)	Time Lag (days)	Duration (days)
ASCA SIS0:				
0.5–8 keV	3.0×10^{17}	0.5	...	0.8
0.5–2 keV	2.0×10^{17}	...	0.06[a]	...
EUVE (50–150 eV).....	4.0×10^{16}	1–2	1[b]	1.5
IUE (1200–2800 Å).....	1.5×10^{15}	3–4	2[b]	2.5

NOTE.—Characteristics of central flare on May 19–21.

[a] Temporal delay with respect to the SIS0 flux in the 2–8 keV band.

[b] Temporal delay with respect to the full-band SIS0 flux (0.5–8 keV), computed from cross-correlations of the UV light curve with the *EUVE* and with the *ASCA* light curves.

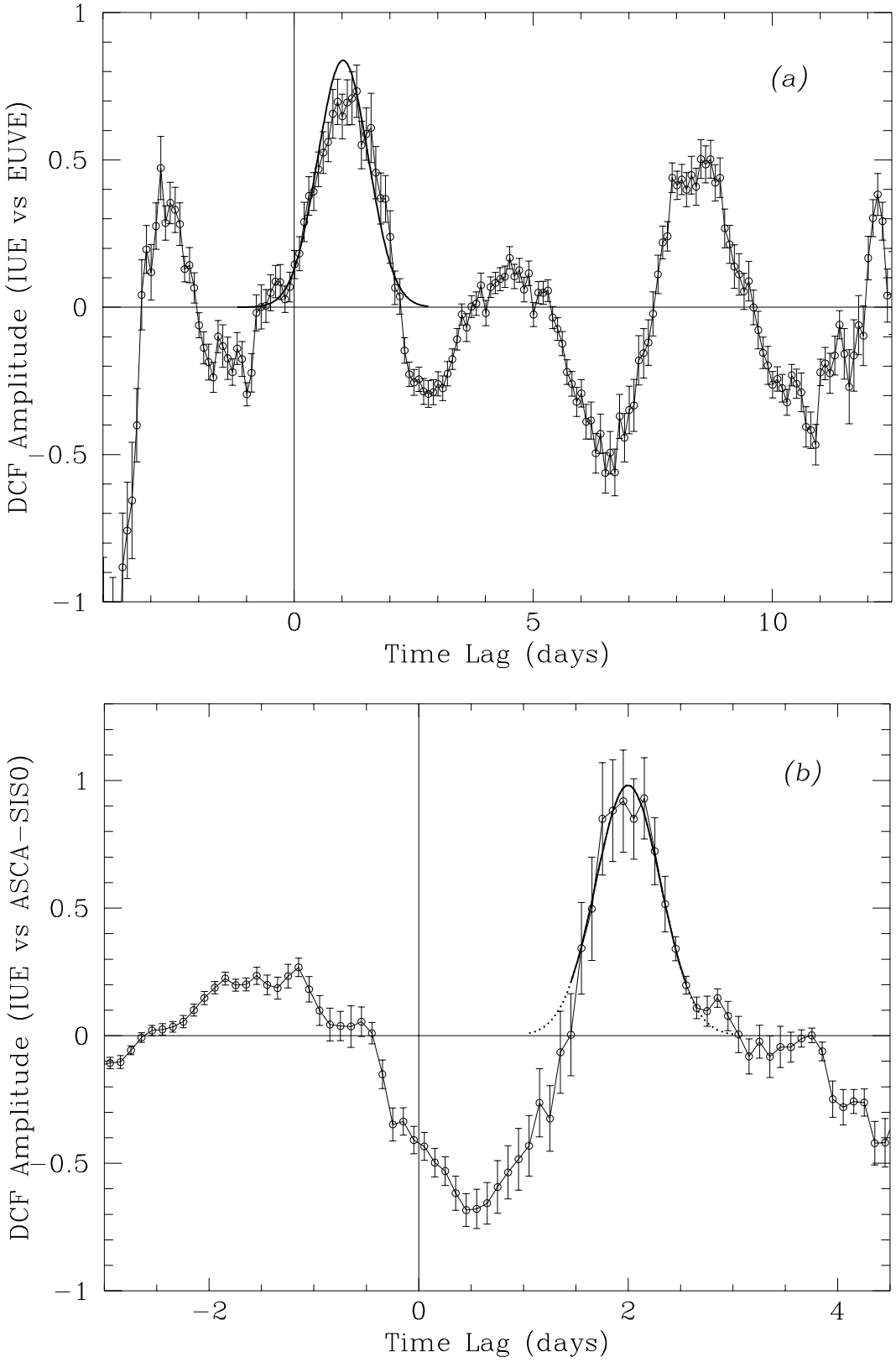

FIG. 3.—Cross-correlation amplitudes obtained with the DCF method. (*a*) *EUVE* flux leads *IUE* flux by ~1 day. (*b*) *ASCA* SIS0 flux leads *IUE* flux by ~2 days. Temporal lags were determined with Gaussian fits to the peaks of the DCFs (*thick solid line*); dotted regions in (*b*) were not included in the fit to the *ASCA-IUE* DCF.

energy distributions (SEDs) that describe the spectral evolution during the correlated multiwavelength flare. The chosen epochs are (1) the "quiescent" period, on May 16.5; (2) at the beginning of the X-ray flare, on May 19.2; (3) at the peak of the X-ray flare, on May 19.4; and (4) at the peak of the UV flare, on May 20.7 (using the closest X-ray data, from 12 hr earlier). The EUV fluxes are strongly dependent upon the assumed $N_{\rm H\,I}$ along the line of sight, so we have

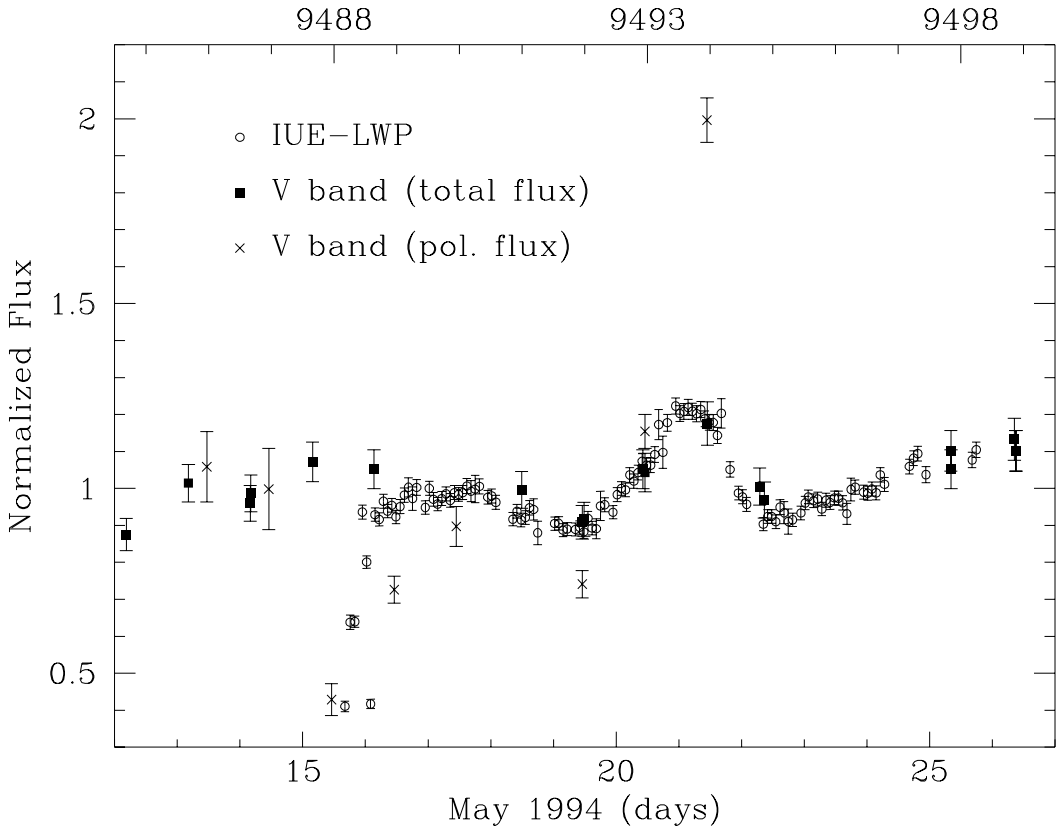

FIG. 4.—Comparison of UV and V-band light curves of PKS 2155−304 in 1994 May, each normalized to its mean. The largest variation is seen in polarized flux, while in total V-band flux the variations are very similar to the UV light curve. No lags were detected with respect to the UV, in part because of the sparse sampling of the optical data; the peaks in the UV flux and the V-band polarization occur within $\sim$1 day. Modified Julian Dates are reported on the upper axis.

plotted points for the best Galactic value, $N_{\rm H\,I} = 1.36 \times 10^{20}$ cm^{-2} (Lockman & Savage 1995), and in parentheses for a value only 0.1×10^{20} cm^{-2} lower, a typical uncertainty on arcminute scales (Elvis, Lockman, & Wilkes 1989). Figure 5 shows that already at the beginning of the X-ray flare the X-ray spectrum hardens, grows in intensity up to the peak, and steepens going back to the preflare intensity while the UV rises. The spectral evolution of the flare shows that the flare power is first injected at high energy and then migrates to lower energies. Note that the peak powers emitted at X-ray and (later) at UV energies are of the same order.

4. DISCUSSION

4.1. *General Considerations for the Synchrotron Model*

In PKS 2155−304 the emission mechanism from the UV through the medium-energy X-ray band is synchrotron radiation, according to many multiwavelength spectral analyses (Edelson et al. 1995, and references therein). This is supported by optical and UV variability (Urry et al. 1993) and particularly by the large and variable polarization at those wavelengths (Smith et al. 1992). The *ASCA* spectrum, with energy spectral index $\alpha \sim 1.3$–1.8 (Kii et al. 1997), is steeper than the UV ($\alpha \sim 1$; Pian et al. 1997), as expected for the high-energy tail of the synchrotron spectrum. It is apparent from Figure 5 that the peak luminosity in the synchrotron component of the spectral energy distribution of PKS 2155−304 falls in the EUV band, corresponding to the definition of a "high-frequency peaked" BL Lac object (Padovani & Giommi 1995).

PKS 2155−304 has been detected with the *Compton Gamma Ray Observatory*'s EGRET instrument with a flat ($\alpha = 0.7 \pm 0.3$) spectrum (Vestrand, Stacy, & Sreekumar 1996) and possibly with OSSE (McNaron-Brown et al. 1995), implying the presence of a separate hard component. This component does not contribute significantly to the *ASCA* spectrum, since no indication of high-energy flattening is found. The OSSE flux greatly exceeds the extrapolations from either EGRET or *ASCA* spectra except for the short-lived flare peak; it may possibly be contaminated by a nearby Seyfert galaxy, NGC 7172.

The spectral energy distribution and the X-ray behavior of PKS 2155−304 closely resemble those of another BL Lac object, Mrk 421. In particular, in Mrk 421 the soft X-ray photons also lag the harder ones by about 2 hr. The gamma-ray emission in both objects can derive from Compton scattering of high-energy electrons off the synchrotron photons (the SSC mechanism; see, e.g., Ghisellini & Maraschi 1996). We also note that Mrk 421 is a strong source of TeV photons and expect that PKS 2155−304 would be detected as a TeV source with a southern array (Stecker, de Jager, & Salamon 1996).

Emission models of blazars require that the observed radiation is Doppler boosted, implying that the emitting plasma moves at relativistic speed. Different emission regions contribute to the low-frequency end (radio to millimeter) of the spectrum, yielding a relatively flat overall energy distribution (e.g., Königl 1989). At higher frequencies the spectrum steepens and could be produced in a single region (homogeneous model), or alternatively, the

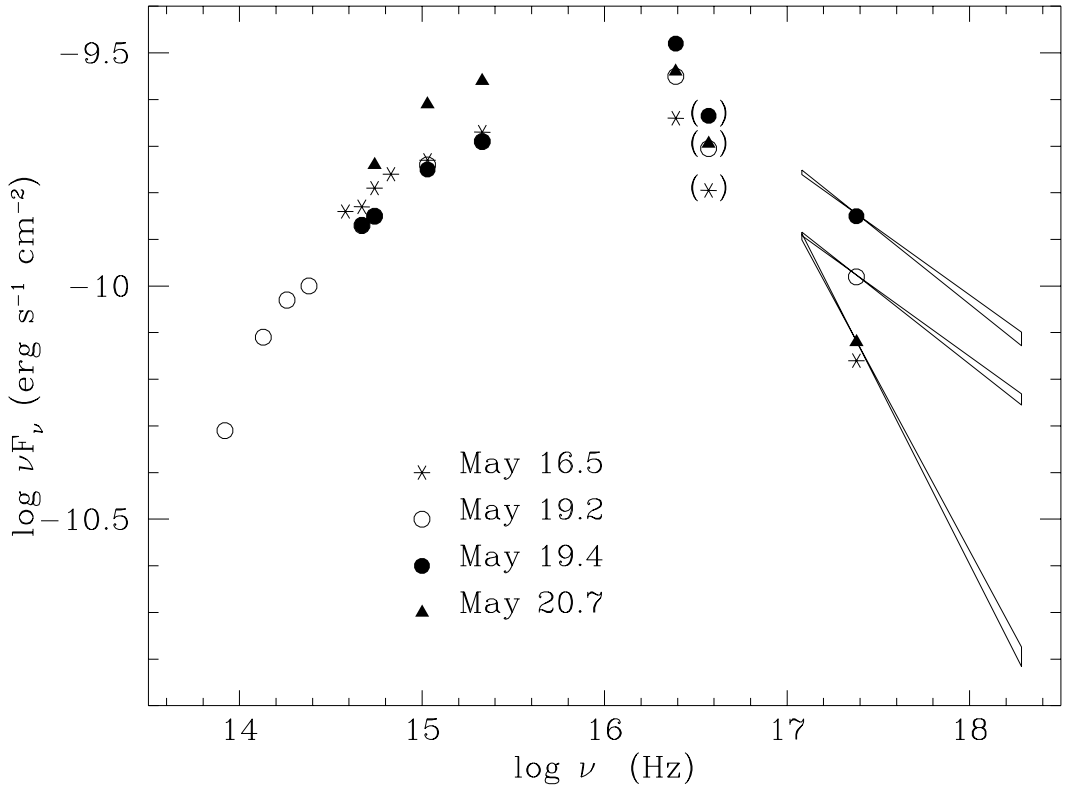

FIG. 5.—Multiwavelength radio through X-ray spectral energy distributions of PKS 2155−304 at four epochs before and through the central flare. The X-ray spectrum clearly softens with decreasing intensity, as the energy appearing initially at X-ray energies is manifested, with approximately the same power, at EUV and then UV wavelengths. The EUV fluxes are strongly dependent upon the assumed $N_{\rm H\,I}$ along the line of sight; points are plotted for the best Galactic value, $N_{\rm H\,I} = 1.36 \times 10^{20}$ cm^{-2} (Lockman & Savage 1995), and in parentheses for a value only 0.1×10^{20} cm^{-2} lower, a typical uncertainty on arcminute scales (Elvis, Lockman, & Wilkes 1989).

steepening of the continuum could be associated with further structure in the jet, in the sense of higher frequencies' being produced closer to the jet core (inhomogeneous jet; Ghisellini, Maraschi, & Treves 1985). The observed SEDs can be explained reasonably well in both cases. However, the homogeneous model is fully constrained if the SED is known up to the gamma-ray range and the variability timescale is taken to infer the size, while the inhomogeneous model has more degrees of freedom. In the following, we discuss the implications of the present results within the two scenarios.

A model-independent conclusion from our data is that the high-energy particles causing the synchrotron flare cannot be produced by a stochastic acceleration process, such as diffusive acceleration at a shock front. Since shock acceleration is a cumulative process, the density of the lower energy particles builds to a maximum first, followed by particles of higher energy, as shown by detailed computations (Fritz & Webb 1990; this calculation neglected Compton losses and applied to a nonrelativistic shock wave). If this type of acceleration process caused the observed flare in PKS 2155−304, the X-ray flare would peak after the UV flare, contrary to what is observed. The data suggest alternative types of acceleration mechanisms, such as acceleration by large-scale electric fields (see, e.g., Bednarek, Kirk, & Mastichiadis 1996a, 1996b). The observed lag of the soft photons with respect to the hard could be caused by particles with initially high energies evolving via energy losses to lower energies (in either the homogeneous or inhomogeneous case), or to inhomogeneous particle distributions affected by a passing disturbance (e.g., a moving shock or compression wave), or to some combination of the two.

4.2. *Homogeneous Models*

The simplest cause of a flare in a homogeneous synchrotron model would be a sudden, uniform increase in the density of energetic electrons. The multifrequency light curves expected from this kind of model need to be calculated in detail, since they depend upon (1) the timescale and spectrum of energy injection, (2) the evolution of the particle spectrum (a balance between acceleration and radiative or other losses), and (3) light-travel time effects. Some spectra have been computed for a limited set of time-dependent particle distributions and applied to Mrk 421 (Mastichiadis & Kirk 1997, neglecting light-travel time effects; Ghisellini & Chiaberge 1997). These imply magnetic fields and Doppler factors very similar to those derived independently from the X-ray lags. Similar calculations should be applied to PKS 2155−304 but are beyond the scope of this paper.

Qualitatively, the observed variations in PKS 2155−304—largest and fastest at the shortest wavelengths—follow the trend expected for the spectral evolution of relativistic electrons suffering radiative losses. Synchrotron (and Compton) losses are energy dependent, with radiating particles having lifetimes inversely proportional to frequency,

$$t_s = 2 \times 10^4 B^{-3/2} \delta^{-1/2} \nu_{15}^{-1/2} \text{ s} \quad (1)$$

(Tucker 1975), where t_s and $\nu_{15} \equiv \nu/(10^{15}$ Hz) are in the observer's frame, B is in gauss, and $\delta \equiv [\gamma(1 - \beta \cos \theta)]^{-1}$ is the Doppler factor.

A soft lag in a uniform model can only arise if lower energy particles derive from initially more energetic ones after substantial energy loss. The injection of particles at high energies must be instantaneous across the volume (relative to the observation timescale) rather than building from lower energies. The increase in high-energy particles must then be balanced by losses such that the X-ray pulse decays before the UV flare rises. The injection cannot occur far above X-ray–emitting energies, since the pulse should broaden as it moves down in energy. Whether this set of constraints can be met by a homogeneous model depends upon detailed calculations not attempted for this paper.

Simple estimates force us to continue to consider the homogeneous case, however. We note that the lag must be of the order of the radiative time at the softer energy and that the lags at different frequencies should approximately satisfy equation (1) above (B is constant by assumption in the homogeneous case). In fact, the lag of 2 days at UV wavelengths, the lag of 1 day at EUV wavelengths, and the lag of 5 ks at soft X-ray wavelengths (all with respect to hard X-rays) are roughly consistent with the prediction of equation (1).

If the observed lag of the soft X-ray photons versus the hard ones is attributed to radiative losses, an estimate of the magnetic field follows. For a Doppler factor $\delta \sim 10$, the observed lags imply $B \sim 0.1$–0.2 G. These values are very similar to those derived for Mrk 421 by Takahashi et al. (1996), which had similar X-ray lags. For Mrk 421, a fit to the broadband spectrum with a homogeneous SSC model requires a Doppler factor of 18 in order not to exceed the observed gamma-ray emission (Ghisellini, Maraschi, & Dondi 1997; Mastichiadis & Kirk 1997). For PKS 2155−304 the required Doppler factor is still higher, close to $\delta \sim 30$ if the (unmeasured) gamma-ray flux at the time of our observations was as bright as that measured by EGRET 6 months later; δ must be even larger if the actual level of gamma-ray emission was lower.

We conclude that a sudden injection of high-energy particles in a uniform region may be a viable explanation of the observed light curves. It does require a very high value of the Doppler beaming factor. More detailed, time-dependent calculations are needed to check whether this scenario is indeed possible.

It appears unlikely that the energy release occurs through a pair cascade, since the spectra computed from pair cascades tend to be very broad (Levinson & Blandford 1995). In contrast, the flare fades in X-rays before rising in the UV, implying a relatively narrow energy distribution at a given time.

4.3. *Inhomogeneous Models*

An alternative way to have the X-ray flare precede the UV is that particles of different energies have different locations along the jet axis. (Note that, at a fixed wavelength, the dominant emission region may still be approximately homogeneous.)

This inhomogeneity could occur behind a shock front, where particles continuously accelerated at the shock fill an energy-dependent volume determined by radiation losses (a "stratified shock"; Marscher 1996). In this case the lags would still be of the order of the radiative lifetimes, so the parameter estimates of the previous section apply. Also, the volume filled by particles of a given energy is related to their radiative lifetimes so that the flare could naturally be symmetric. The requirement on the Doppler factor could be somewhat relaxed since there are larger volumes for the lower energy particles. A quantitative model should be computed to assess this case.

A different scenario is that of an inhomogeneous jet, where the particle energy distributions change along the jet as a result of a local balance between acceleration and energy-loss processes. The main difference between the two pictures is that, in the first case, particle acceleration is localized at the shock front while, in the second, it occurs throughout the jet volume. In both cases, spectral steepening from UV to X-rays is due to the diminishing volumes occupied by particles of higher energies.

A disturbance crossing a steady state shock front or propagating along an inhomogeneous jet would affect the higher energy particles first and extend gradually to the larger region occupied by the lower energy particles. The "thickness" of the disturbance (its length) should be comparable to or larger than the size of the X-ray–emitting region, or else the amplitude of the X-ray flare would be smaller (and indeed not significantly advanced with respect to the UV).

The radiative lifetimes can be very short in this scenario, and variability timescales are associated with the travel time of the disturbance through the emission region. This is comparable to the light-travel time if the disturbance is a relativistic shock wave propagating in the same direction as the jet flow. The predicted variability for this kind of model (Celotti et al. 1991) agrees qualitatively with the variability observed in PKS 2155−304. The duration of the pulse is related to the size of the emission region at that wavelength, and in typical models the UV-emitting region is larger than the EUV, which is larger than the X-ray. The delay between X-ray, EUV, and UV emission would correspond to the linear distance between the centers of the respective emission regions. We note that the observed delays are of the same magnitude as the duration of the flare, as expected if the disturbance moves smoothly from X-ray– to EUV- to UV-emitting regions.

It is beyond the scope of this paper to fit specific time-dependent inhomogeneous models to the flare's evolution. We do note that this kind of model can have a stronger magnetic field than the homogeneous case, because it is not dictated by the observed timescales; thus, inhomogeneous models can account for the average SED, including the gamma rays, with a lower value of the Doppler beaming factor.

4.4. *Contrast to Variability of PKS 2155−304 in 1991 November*

The light curves obtained in 4.5 days of monitoring of PKS 2155−304 in 1991 November (Edelson et al. 1995) are substantially different from those discussed here. The amplitude of variability in 1991, from X-ray to UV to optical, was considerably smaller, with $\sim 10\%$ variations in single flares and an overall $\sim 30\%$ decline in intensity, and was independent of wavelength. Equally striking, the X-ray flux led the UV by no more than 2 hr.

The close correlation of optical and UV light curves in 1991 ruled out substantial contribution from an accretion disk, and the close correlation of all the light curves sup-

ported the notion of a common origin for the emission, quite plausibly synchrotron emission. However, the constraints on models that would be derived from the 1991 data would be entirely different from those implied by the 1994 data. That is, either the variability is caused by some second mechanism or the parameters of the emitting region have changed considerably.

In the spirit of our general discussion, we consider briefly the former possibility. Because the 1991 variability was achromatic, which is not natural for intrinsic changes in a synchrotron emitter, it may be extrinsic. Specifically, it could be caused by microlensing by stars in an intervening galaxy (Treves et al. 1997). There is a strong Lyα absorption system at a favorable location for lensing ($z = 0.059$; Bruhweiler et al. 1993), roughly halfway to PKS 2155−304 ($z = 0.116$; Falomo, Pesce, & Treves 1993). If the size of the emission region does not depend strongly upon wavelength, then microlensing can cause achromatic variations (Schneider & Weiss 1987; Kayser et al. 1989). The apparent relativistic motion of the jet with respect to the lensing stars can cause timescales as short as those observed in PKS 2155−304 (Gopal-Krishna & Subramanian 1991). The a priori probability of detecting a microlensing event during the 1991 campaign was estimated by Treves et al. (1997) to be a few percent, small but not negligible.

Alternatively, it was suggested (Urry et al. 1993) that the 1991 variability could be associated with helical trajectories of moving knots in a relativistic jet (Camenzind & Krockenberger 1992), that is, due essentially to a change in viewing angle. Such an explanation could not cause the strong wavelength dependence of the variations seen in 1994 May.

5. CONCLUSIONS

We have obtained multiwavelength light curves of unprecedented coverage and time resolution for any blazar. The emission at X-ray, EUV, and UV wavelengths is well correlated but with significant delays of approximately 1–2 days, and the soft X-ray photons lag the hard by about ~1–2 hr. These lags approximately satisfy a $\nu^{-1/2}$ relation, suggesting they are related to radiative losses.

The apparent progression of a strong X-ray flare to longer wavelengths rules out a stochastic acceleration process in a homogeneous volume. It can possibly be explained by an instantaneous injection of high-energy particles near X-ray–emitting energies and subsequent energy degradation in a homogeneous radiating synchrotron source. This injection could be achieved by a single-stage acceleration, as with a large-scale electric field (Bednarek et al. 1996a, 1996b). A radiative interpretation of the observed lags then constrains the magnetic field to be rather low and requires a very high value of the Doppler beaming factor ($\delta \sim 30$) in order not to exceed the highest gamma-ray flux observed (not simultaneously) with EGRET. Such a homogeneous model may be finely tuned but cannot be ruled out with present data. The estimated physical parameters are similar to those derived with the same assumptions from similar data for the BL Lac object Mrk 421 (Takahashi et al. 1996).

In contrast, an inhomogeneous jet model incorporating acceleration by shocks can represent both the broadband spectrum and the observed spectral evolution of the flare, with a higher magnetic field. The cause of the flare in this model is a propagating disturbance affecting different regions at different times. The flatter X-ray spectra during the rise of the flare can be accounted for with an increase in the cutoff energy of the electron spectrum at the site of the perturbation, possibly due to shock acceleration. A stratified shock model provides an acceptable manifestation of the inhomogeneous case but requires the timescales to be close to the radiative lifetimes of the particles, as in the homogeneous model. An energy-dependent volume does, however, relax somewhat the constraints on the Doppler beaming factor.

The different multifrequency behavior observed in 1991 indicates that different mechanisms of variability can operate in this source. It is important to confirm that at least large flares have a qualitatively constant behavior. In particular, the lags should not change substantially in the homogeneous energy degradation model.

C. M. U., J. E. P., and E. P. acknowledge support from NASA grants NAG 5-1034 and NAG 5-2499, and E. P. acknowledges the support of a NATO-CNR Advanced Fellowship. Some of this work was completed while L. M. was at STScI courtesy of the STScI Visitor Program. R. M. S. acknowledges support from an NRC Research Associate Fellowship.

REFERENCES

Ayres, T. R. 1993, PASP, 105, 538
Ayres, T. R., et al. 1995, ApJS, 96, 223
Bednarek, W., Kirk, J. G., & Mastichiadis, A. 1996a, A&A, 307, L17
———. 1996b, A&AS, 120, 571
Bregman, J. N., Maraschi, L., & Urry, C. M. 1987, in Exploring the Universe with the *IUE* Satellite, ed. Y. Kondo & W. Wamsteker (Dordrecht: Reidel), 685
Brinkmann, W., et al. 1994, A&A, 288, 433
Bruhweiler, F. C., Boggess, A., Norman, D. J., Grady, C. A., Urry, C. M., & Kondo, Y. 1993, ApJ, 409, 199
Camenzind, M., & Krockenberger, M. 1992, A&A, 255, 59
Celotti, A., Maraschi, L., & Treves, A. 1991, ApJ, 377, 403
Courvoisier, T. J.-L., et al. 1995, ApJ, 438, 108
Dermer, C. D., & Schlickeiser, M. 1993, ApJ, 416, 458
Edelson, R. A., & Krolik, J. H. 1988, ApJ, 333, 646
Edelson, R. A., et al. 1995, ApJ, 438, 120
Elvis, M., Lockman, F. J., & Wilkes, B. J. 1989, AJ, 97, 777
Falomo, R., Pesce, J. E., & Treves, A. 1993, ApJ, 411, L63
Fritz, K., & Webb, G. M. 1990, ApJ, 360, 387
Fruscione, A., Bowyer, S., Königl, A., & Kahn, S. 1994, ApJ, 422, L55
Ghisellini, G., & Chiaberge, M. 1997, Mem. Soc. Astron. Italiana, in press
Ghisellini, G., & Maraschi, L. 1996, in ASP Conf. Ser. 110, Blazar Continuum Variability, ed. H. R. Miller, J. R. Webb, & J. C. Noble (San Francisco: ASP), 436
Ghisellini, G., Maraschi, L., & Dondi, L. 1997, A&A, in press
Ghisellini, G., Maraschi, L., & Treves, A. 1985, A&A, 146, 204
Giommi, P., Ansari, S. G., & Micol, A. 1995, A&AS, 109, 267
Gopal-Krishna & Subramanian, K. 1991, Nature, 349, 766
Kayser, R., Weiss, A., Refsdal, S., & Schneider, P. 1989, A&A, 214, 4
Kii, T., et al. 1997, in preparation
Kinney, A. L., Bohlin, R. C., & Neill, J. D. 1991, PASP, 103, 694
Königl, A. 1989, in Lecture Notes in Physics, 334, BL Lac Objects, ed. L. Maraschi, T. Maccacaro, & M.-H. Ulrich (Berlin: Springer), 321
Königl, A., Kartje, J. F., Bowyer, S., Kahn, S. M., & Hwang, C.-Y. 1995, ApJ, 446, 598
Levinson, A., & Blandford, R. D. 1995, ApJ, 449, 86
Lockman, F. J., & Savage, B. D. 1995, ApJS, 97, 1
Maraschi, L., Ghisellini, G., & Celotti, A. 1992, ApJ, 397, L5
———. 1994, in IAU Symp. 159, Multi-Wavelength Continuum Emission of AGN, ed. T. J.-L. Courvoisier & A. Blecha (Dordrecht: Kluwer), 221
Marscher, A. P. 1996, in ASP Conf. Ser. 110, Blazar Continuum Variability, ed. H. R. Miller, J. R. Webb, & J. C. Noble (San Francisco: ASP), 248
Marshall, H. L., et al. 1997, in preparation
Mastichiadis, A., & Kirk, J. G. 1997, A&A, 320, 19
McNaron-Brown, K., et al. 1995, ApJ, 451, 575
Padovani, P., & Giommi, P. 1995, ApJ, 444, 567
Pesce, J. E., et al. 1997, ApJ, 486, 770
Pian, E., et al. 1997, ApJ, 486, 784

Sambruna, R. M., Barr, P., Giommi, P., Maraschi, L., Tagliaferri, G., & Treves, A. 1994, ApJ, 434, 468
Sambruna, R. M., Maraschi, L., & Urry, C. M. 1996, ApJ, 463, 444
Schneider, P., & Weiss, A. 1987, A&A, 171, 49
Sembay, S., Warwick, R. S., Urry, C. M., Sokoloski, J., George, I. M., Makino, F., & Ohashi, T. 1993, ApJ, 404, 112
Smith, P. S., Hall, P. B., Allen, R. G., & Sitko, M. L. 1992, ApJ, 400, 115
Stark, A. A., Gammie, C. F., Wilson, R. W., Bally, J., Linke, R. A., Heiles, C., & Hurwitz, M. 1992, ApJS, 79, 77
Stecker, F. W., de Jager, O. C., & Salamon, M. H. 1996, ApJ, 473, L75
Takahashi, T., et al. 1996, ApJ, 470, L89
Tanaka, Y., Inoue, H., & Holt, S. S. 1994, PASJ, 46, L37
Treves, A., Jetzer, P., Rovetti, F., & Urry, C. M. 1997, in Proc. Girona Conf., Blazars, Black Holes, and Jets (Dordrecht: Kluwer), in press
Treves, A., et al. 1989, ApJ, 341, 733
Tucker, W. 1975, Radiation Processes in Astrophysics (Cambridge: MIT Press)
Urry, C. M., et al. 1993, ApJ, 411, 614
Vestrand, W. T., Stacy, J. G., & Sreekumar, P. 1996, ApJ, 454, L93
von Montigny, C., et al. 1995, ApJ, 440, 525